

Dosimetric dependence of the dimensional characteristics on a lead shield in electron radiotherapy: a Monte Carlo study

James C L Chow^{1a,2,3} and Grigor N Grigorov⁴

*Radiation Medicine Program,¹ Princess Margaret Hospital and Department of Radiation Oncology, University of Toronto, Toronto, Ontario, Canada; Department of Physics,² University of Waterloo, Waterloo, Ontario, Canada; Department of Physics,³ Ryerson University, Toronto, Ontario, Canada; Medical Physics Department,⁴ Grand River Regional Cancer Center, Kitchener, Ontario, Canada.
james.chow@rmp.uhn.on.ca*

Received 1 August, 2008; accepted 18 November, 2008

This study investigates the dosimetric dependence of the dimension of a lead (Pb) layer for shielding using clinical electron beams with different energies. Monte Carlo simulations were used to generate phase space files for the 4, 9 and 16 MeV electron beams produced by a Varian 21 EX linear accelerator using the EGSnrc-based BEAMnrc code, and validated by measurements using films. Pb layers with different thicknesses (2, 4, 6 and 8 mm) and diameters (2.5, 3, 3.5 and 4 cm) were placed at the center of an electron field on a solid water phantom. Beam profiles were determined at the depth of maximum dose (d_m) using Monte Carlo simulations. The dose profiles under the Pb layer at d_m , including the penumbra at the edge of the layer and relative dose at the central beam axis (CAX), were studied with varying thicknesses and diameters of Pb. It is found that 2 mm of Pb is adequate to provide 5 half value layer (HVL) attenuation for the 4 MeV electron beams, and the beam profiles at d_m are dependent on the diameter but not the thickness of the Pb. However, for the 9 and 16 MeV electron beams, the relative dose at the CAX and d_m depends on both the thickness and diameter of the Pb layer. For 8 mm thickness of Pb, 4 and 5 HVL attenuation of electron beams with energies of 9 and 16 MeV can be achieved at d_m , respectively. Moreover, the beam profile under the Pb layer at d_m depends on: (1) the penumbra region at the edge of the Pb layer; (2) the beam attenuation varying with the thickness of the Pb layer; (3) the electron side scatter contributing to the CAX under the Pb layer; and (4) the photon contamination produced by the Pb layer. A parameter called “shielding area factor” (defined as the ratio of the length between two points of 50% relative doses in the beam profile at d_m to the diameter of the Pb layer) is suggested to predict the required size and thickness of Pb for shielding a target with known dimension at d_m . The dosimetric data calculated by Monte Carlo simulations in this study are useful to select the suitable thickness and size of Pb for the protection of critical tissue in electron radiotherapy.

PACS number: 87.53.Bn; 87.55.kh and 87.55.km.

Key words: electron radiotherapy, Monte Carlo, Pb shielding, electron dosimetry

I. INTRODUCTION

In electron radiotherapy, superficial lesions on the eye or eyelid can be treated by low-energy electron beams (4 - 9 MeV). To protect critical structures such as the lens during treatment,

^a Corresponding author: Dr James Chow, Department of Radiation Physics, Princess Margaret Hospital, University Health Network, 610 University Avenue, Toronto, Ontario, Canada M5G 2M9; phone: 416 946 4501; fax: 416 946 6566; email: james.chow@rmp.uhn.on.ca

lead (Pb) is used as shielding.⁽¹⁾ A patient-specific electron cutout inserted in the bottom of an electron applicator is used together with a layer of Pb (or commercially available eye shield made of Pb or tungsten (W)) placed on the patient surface.^(2,3) In this treatment setup and geometry, there are several dosimetric concerns about the dose distribution at the prescription depth or depth of maximum dose (d_m). One of the common concerns is the dose enhancement to the critical tissue due to the electron backscatter from the Pb shield.^(1,4,5) There have been many studies regarding Monte Carlo simulations or measurements using TLD, films, metal-oxide-semiconductor field effect transistor (MOSFET), and plane parallel ionization chamber on the electron backscatter from Pb irradiated by photon and electron beams.^(1,4,5-11) Other studies of electron backscatter focused on commercial eye shields made of either Pb or W.^(2,3) A more general approach using different thicknesses of Pb layers was used in this study to determine the dosimetry of backscatter at the Pb-tissue interface.

Results of Monte Carlo simulations studying the dependences of the electron backscatter on the beam obliquity, energy, thickness of Pb, and depth of the Pb-tissue interface using the EGSnrc-based code have recently been published.⁽¹¹⁾ In addition, the relatively new MOSFET dosimeter was examined to determine the electron-backscattered dose accurately at the Pb-tissue interface.^(12,13) However, related studies concerning the effect of the dimensions of the Pb layer on the dose distribution under the Pb shield (at the prescription depth or d_m) is lacking. The dosimetry near the d_m and build-up region for the low-energy electron beam (i.e. 4 MeV) is more complex compared to higher energies due to the larger angular scattering cross-section and shorter effective range.^(14,15) In addition, when the Pb layer is placed on the patient/phantom surface under the electron applicator with cutout, the dosimetry in the penumbra regions and central beam axis (CAX) of the beam profile depends on the dimensional characteristics of the Pb layer, such as its diameter and thickness. The aim of this study is to determine the dosimetric characteristics such as the beam profile, relative dose at the CAX and penumbra width at d_m with varying diameters and thicknesses of the Pb layer and different electron beam energies.

To determine this new dosimetric data for the Pb shield, Monte Carlo simulations, validated by measurements, were used to calculate the beam profiles at d_m for different Pb shields and electron beam energies. The advantages of using Monte Carlo simulations instead of measurements to determine the dose distributions are: (1) minimizing the time and effort needed in measuring the beam profiles with a scanning water tank since only measurements for validation are needed; (2) avoiding human error in the experimental setup and fabrications of cutouts and Pb layers in the measurement; and (3) simulation results account for the electron scattering for the low-energy electron beam and electron disequilibrium effect for the high-energy electron beam.⁽¹⁶⁾

In this study, electron beams with energies of 4, 9 and 16 MeV produced by a Varian 21 EX linear accelerator (Linac) were used. Although low-energy electron beams were used to treat superficial lesions, dosimetric data of the 16 MeV electron beams were calculated here for a more thorough analysis and comparison. Kodak XV radiographic film was used to validate Monte Carlo simulations.

II. MATERIALS AND METHODS

A. Experimental Setup

The experimental setup and geometry for studying the dosimetry at the prescription depth or d_m can be seen in Fig. 1. Pb layers with thicknesses ranging from 2 – 8 mm were placed on a solid water slab ($30 \times 30 \text{ cm}^2$) with source-to-surface distance (SSD) = 100 cm. Four sizes of Pb layers with diameters equal to 2.5, 3, 3.5 and 4 cm were used on the phantom surface. The 4, 9 and 16 MeV electron beams produced by the Varian 21 EX Linac with $10 \times 10 \text{ cm}^2$ applicator and circular cutout (diameter = 10 cm) were used in the measurement. Beam profiles at d_m (i.e. 0.7 cm for 4 MeV, 2.2 cm for 9 MeV, and 3 cm for 16 MeV) were calculated using Monte Carlo simulations (EGSnrc-based code) after validations by film measurements.

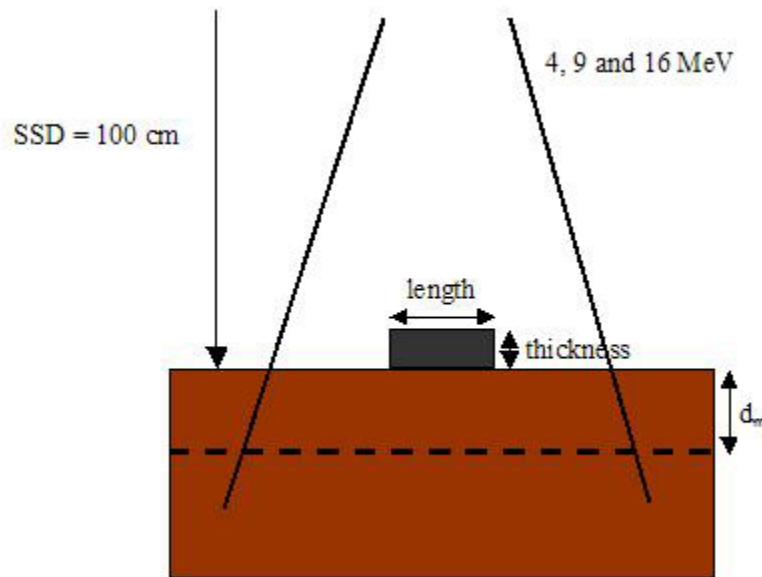


FIG. 1. Schematic diagram showing the experimental setup for Monte Carlo simulations to calculate the beam profiles at d_m (broken line) for the 4, 9 and 16 MeV electron beams. The SSD was equal to 100 cm. The diameters (lengths) and thicknesses of Pb layers were varied from 2.5 – 4 cm and 2 – 8 mm, respectively.

B. Monte Carlo Simulation

The beam profiles for the experimental geometry and setup, as shown in Fig. 1, were calculated using the EGSnrc Monte Carlo code.^(17,18) The BEAMnrc^(19,20) and DOSXYZnrc⁽²¹⁾ code were used to calculate the phase space file for the electron beams and dose in the phantom, respectively.

B.1. Phase Space File for the Electron Beam

Phase space files of the types, positions, energies, and directions of particles for the electron beams with energies of 4, 9 and 16 MeV were generated using the BEAMnrc code (version 4-r2-2-4). The $10 \times 10 \text{ cm}^2$ applicator and circular cutout were used in the phase space file. The initial mean energy (E_0) of the electron beam with SSD = 100 cm produced by the Linac was estimated using the measured electron range at 50% of depth dose (R_{50}) in the commissioning. The following equation relating E_0 and R_{50} was used:⁽²²⁾

$$E_0 = C_4 \times R_{50} \quad (1)$$

Original recommendations by the AAPM TG-21 protocol suggested a value for C_4 of 2.33 MeV/cm for water.⁽²³⁾ However, in the clinical energy range of 1 – 50 MeV, Monte Carlo calculations using EGS4 show that $C_4 = 2.4 \text{ MeV/cm}$.^(24,25) The primary electron energy was estimated by comparing the percentage depth dose (PDD) calculated by the assumed monoenergetic energy of the primary electron using Monte Carlo simulation and the measurement. In this study, the primary electron energies for the 4, 9 and 16 MeV beams were estimated to be 4.17, 10.40 and 17.51 MeV, respectively, with deviation of the PDD between the Monte Carlo simulation and measurement $< \pm 2\%$, after iterative readjustment of the primary electron energies.^(16,26)

In our Monte Carlo simulation, the phase space file (containing at least 10 million particles) was not recycled more than five times when running DOSXYZnrc.⁽²¹⁾ The recycling of a particle does not introduce any bias, as long as the statistical weight and the variance are accurately calculated. The Parameter Reduced Electron Step Transport Algorithm II (PRESTA II) was

used as the electron-step algorithm with the user-adjustable parameters set at their default values.^(27,28) The parameters of the electron cutoff energy (ECUT) and maximum fractional energy loss per electron step (ESTEPE) were set to 700 keV and 0.25, respectively.⁽¹¹⁾

B.2. Dose Calculation With the Pb Layer

The beam profiles in the in-plane or x-axis according to Fig. 1 were calculated using the EGSnrc-based DOSXYZnrc code. The solid water phantom and beam setup in Fig. 1 were input to the DOSXYZnrc with voxel volume equal to $0.2 \times 0.2 \times 0.1 \text{ cm}^3$ for the x, y and z direction, respectively. For electron beams with energies of 4, 9 and 16 MeV, different diameters (2.5, 3, 3.5 and 4 cm) and thicknesses (2, 4, 6 and 8 mm) of Pb layers were placed at the center of a circular field with diameter equal to 10 cm. The space between the applicator and the phantom surface was 5 cm and the SSD (phantom surface) was set to 100 cm. Each simulation was finished using 50 million histories. Under this calculation tally, the relative statistical dose error (that is the uncertainty as a fraction of dose in the voxel) was around $\pm 1\%$ for all electron beam energies.⁽²¹⁾ The parameter of ECUT for DOSXYZnrc was set to 521 keV. The computing time was about 0.5 – 1 hour using a single AMD Athlon 64 X2 4200+ processor with 1 GB RAM.

C. Measurement for Validation of Monte Carlo Simulation

Dose measurements were carried out using Kodak XV films with experimental setup in Fig. 1 to determine the beam profiles at d_m . The film was calibrated with electron beam energies (4, 9 and 16 MeV) produced by the Linac using the standard $10 \times 10 \text{ cm}^2$ applicator and cutout. The absolute dose of 1 cGy per monitor unit (MU) for the electron beam was calibrated by a plane parallel ionization chamber (PTW 23343 Markus) placed at the depth of reference (d_{ref}) in a water tank at SSD = 100 cm using the AAPM TG-51 protocol.⁽²⁹⁾ The absolute dose point was then cross-calibrated with a Farmer-type ionization chamber (CAPINTEC PR-06C) and solid water phantom for the same beam and setup geometry. The solid water slab (CNMC, Tennessee, USA) is designed for photon and electron beam calibration with its mass and volume electron densities, electron and photon transmission characteristics, and with physical dimensions virtually the same as those in liquid water.

For the film calibration, films taken from the same batch were placed in the solid water phantom at d_{ref} (SSD = 100 cm). Different MUs, in the film linear dose sensitivity range (0 - 1 Gy), were used to expose the film for the 4, 9 and 16 MeV electron beams. The exposed films were developed in a Kodak X-Omat 2000 film processor and analyzed using the Vidar VX-16 densitometer with RIT 113 radiation therapy dosimetry software, version 4 (Radiological Imaging Technology, Inc., Colorado Springs, CO, U.S.A.). The sensitometric curve fitting was done by the piecewise polynomial routine in the software. The uncertainty of the film dosimetry is within $\pm 3\%$.⁽³⁰⁾ The measured results using films were used to validate Monte Carlo simulations.

III. RESULTS

Figure 2 shows the beam profiles at d_m for both measured and calculated data using films and Monte Carlo simulations as outlined in the experimental setup in Fig. 1. The diameter of the Pb layer was equal to 2.5 cm and the thickness of the layer was equal to 2, 4 and 6 mm for the electron beams with energies of 4 MeV (Fig. 2(a)), 9 MeV (Fig. 2(b)) and 16 MeV (Fig. 2(c)), respectively. All beam profiles in Fig. 2 were normalized to the maximum doses. It can be seen that the doses calculated by Monte Carlo simulations agree well with the measurements, and therefore the Monte Carlo model for the Linac was verified.

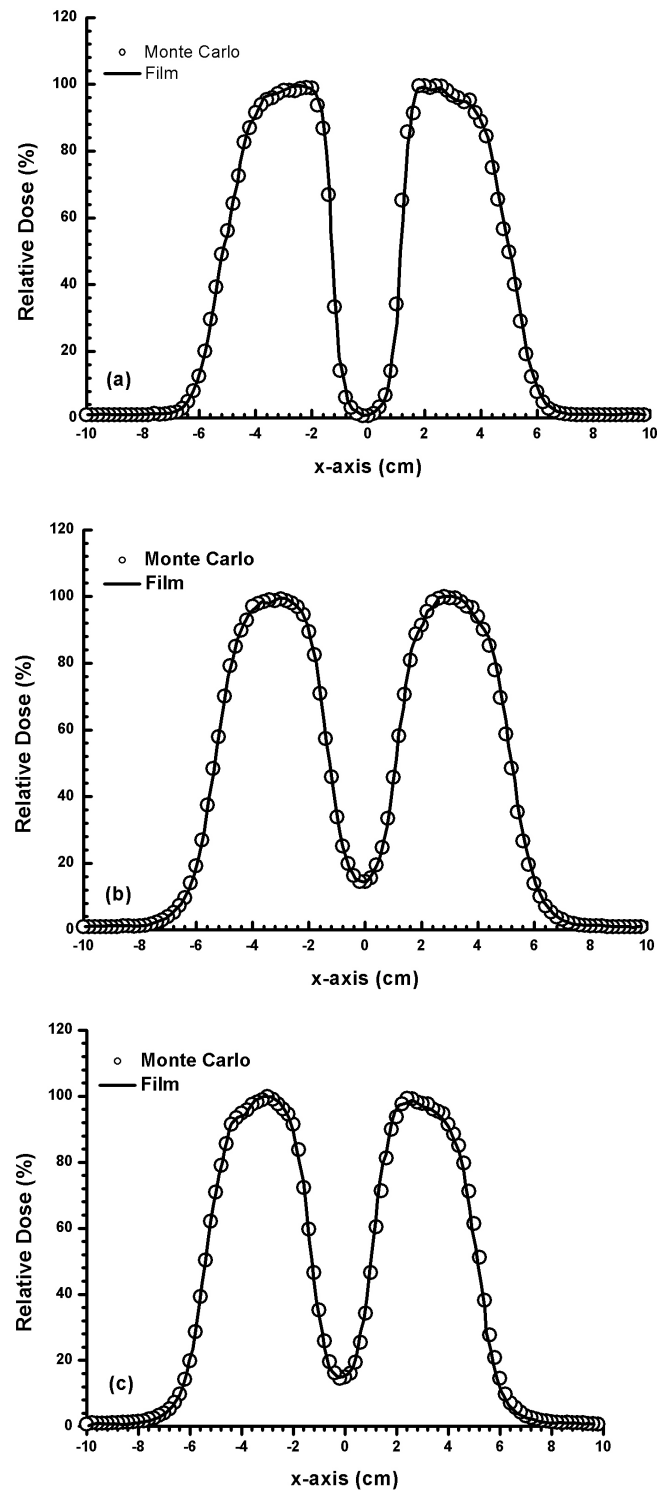


FIG. 2. Beam profiles measured and calculated using films and Monte Carlo simulations for: (a) 4 MeV electron beams with 2 mm thickness of Pb at depth = 0.7 cm, (b) 9 MeV electron beams with 4 mm thickness of Pb at depth = 2.2 cm, and (c) 16 MeV electron beams with 6 mm thickness of Pb at depth = 3 cm. The diameter of the Pb layer was equal to 2.5 cm and experimental setup as in Fig. 1 was used.

Figures 3(a) and 3(b) show the beam profiles at d_m for 2 and 4 mm thickness of Pb with different diameters (2.5, 3, 3.5 and 4 cm) using the 4 MeV electron beam. Figures 4 and 5 show beam profiles with similar experimental setup as in Fig. 3, with electron beam energies of 9 MeV and 16 MeV and thicknesses of 6 and 8 mm of Pb. Thicker Pb layers used in Figs. 4 and 5 were due to the increase of electron beam energy.

Figures 6(a) and 6(b) show beam profiles for Pb layers with diameters of 2.5 and 4 cm using the 4 MeV electron beam. The thicknesses of Pb used were 2, 4, 6 and 8 mm. Figures 7 and 8 show beam profiles for Pb layers similar to Fig. 6, except the electron beam energy was changed to 9 MeV and 16 MeV. The statistical uncertainties for beam profiles in Figs. 3 - 8 calculated using Monte Carlo simulations are within $\pm 1\%$, as discussed in Section II.B.2 above.

Figure 9 shows the relative dose at the CAX for the 2 and 8 mm thicknesses of the Pb using the 4, 9 and 16 MeV electron beams, where the diameter of the Pb layer was equal to 2.5 cm. Figure 10 shows the penumbra width (20% - 80%) under the edge of the Pb layer vs. its diameter at d_m for the 4, 9 and 16 MeV electron beams. In Fig. 10, the thickness of Pb layers for the 4, 9 and 16 MeV electron beams was 2 mm.

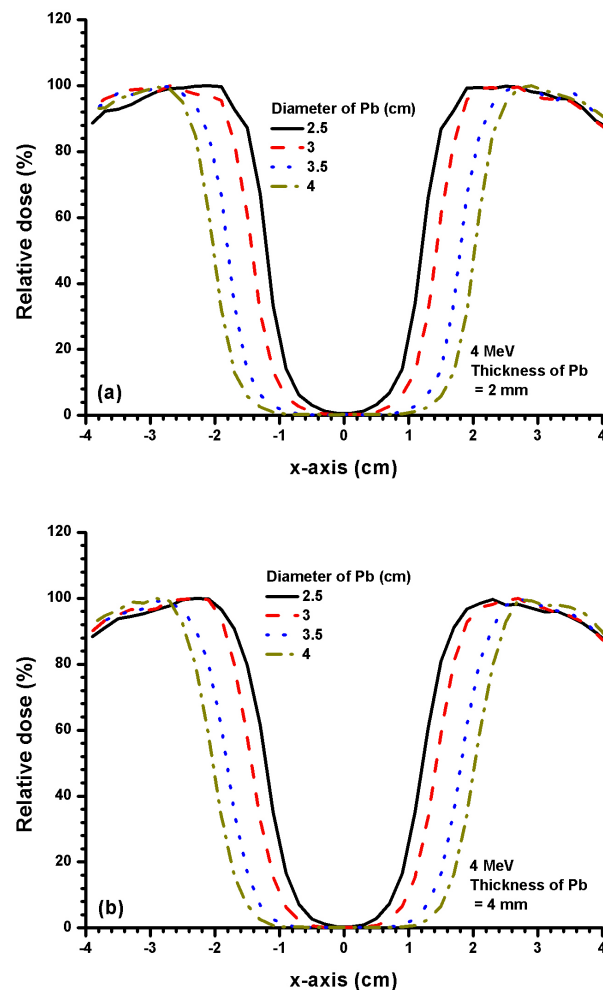


FIG. 3. Beam profiles for Pb layers with diameters of 2.5, 3, 3.5 and 4 cm and thicknesses of (a) 2 mm, and (b) 4 mm. The 4 MeV electron beams with the $10 \times 10 \text{ cm}^2$ applicator and circular cutout were used. It can be seen that both 3(a) and 3(b) had relative doses at the CAX equal to zero.

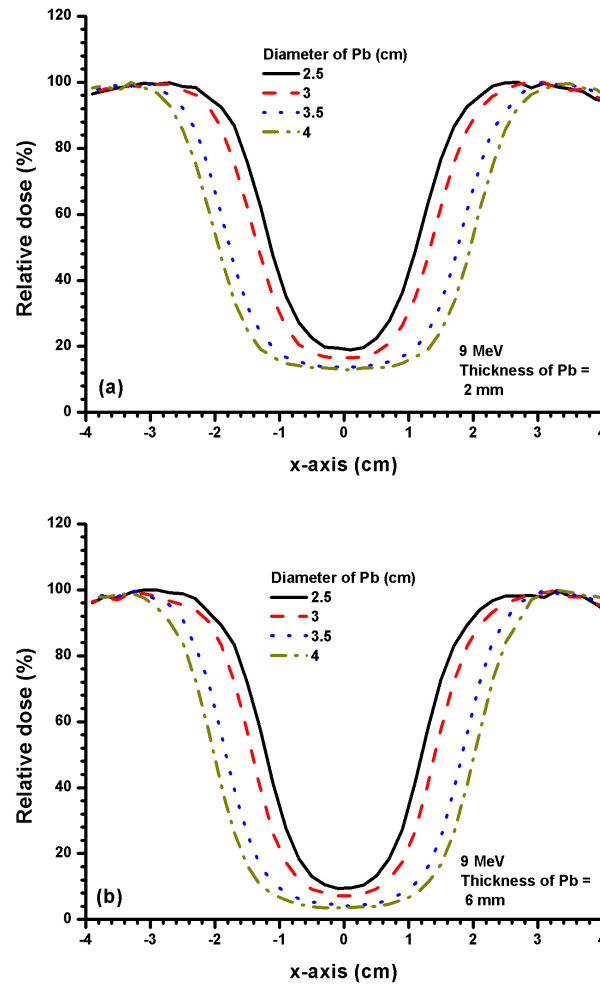


FIG. 4. Beam profiles for Pb layers with diameters of 2.5, 3, 3.5 and 4 cm and thicknesses of (a) 2 mm, and (b) 6 mm. The 9 MeV electron beams with the $10 \times 10 \text{ cm}^2$ applicator and circular cutout were used. The relative dose at CAX in 4(a) decreased from 19.5% to 13.0% when diameter of the Pb layer increased from 2.5 to 4 cm. In 4(b), the relative dose at the CAX decreased from 9.13% to 3.4% when the diameter of the Pb layer increased from 2.5 to 4 cm.

A parameter called the shielding area factor, reflecting the shielding area efficiency of the Pb layer at d_m , was defined in this study. The shielding area factor is defined as:

$$\text{Shielding area factor} = \frac{l(d_m, D_{50\%})}{\text{Diameter of Pb shield}} \quad (2)$$

where l is the length between two points of 50% relative dose ($D_{50\%}$) in the beam profile at d_m . The ratio of l to the physical length (diameter) of the Pb layer/shield on the patient/phantom surface gives the shielding area factor. The changes in shielding area factor with different thicknesses and diameters of Pb layers for the 4 MeV (5 half value layer (HVL) attenuation), 9 MeV (3 and 4 HVL attenuation), and 16 MeV (3 HVL attenuation) electron beams are shown in Tables 1(a), 1(b, c), and 1(d), respectively. The diameter of the Pb layer was equal to 2.5 cm in the table.

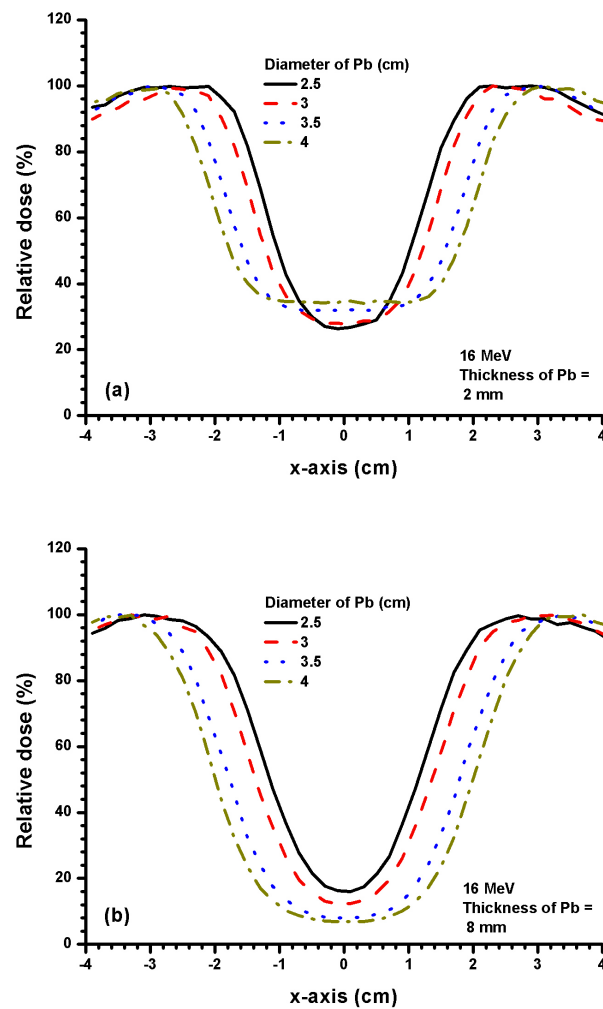


FIG. 5. Beam profiles for Pb layers with diameters of 2.5, 3, 3.5 and 4 cm and thicknesses of (a) 2 mm, and (b) 8 mm. The 16 MeV electron beams with the $10 \times 10 \text{ cm}^2$ applicator and circular cutout were used. The relative dose at the CAX for 5(a) increased from 26.7% to 34.5% when the diameter of the Pb layer increased from 2.5 to 4 cm. The relative dose at the CAX for 5(b) decreased from 15.8% to 6.9% with the same increase of diameter of the Pb layer as in 5(a).

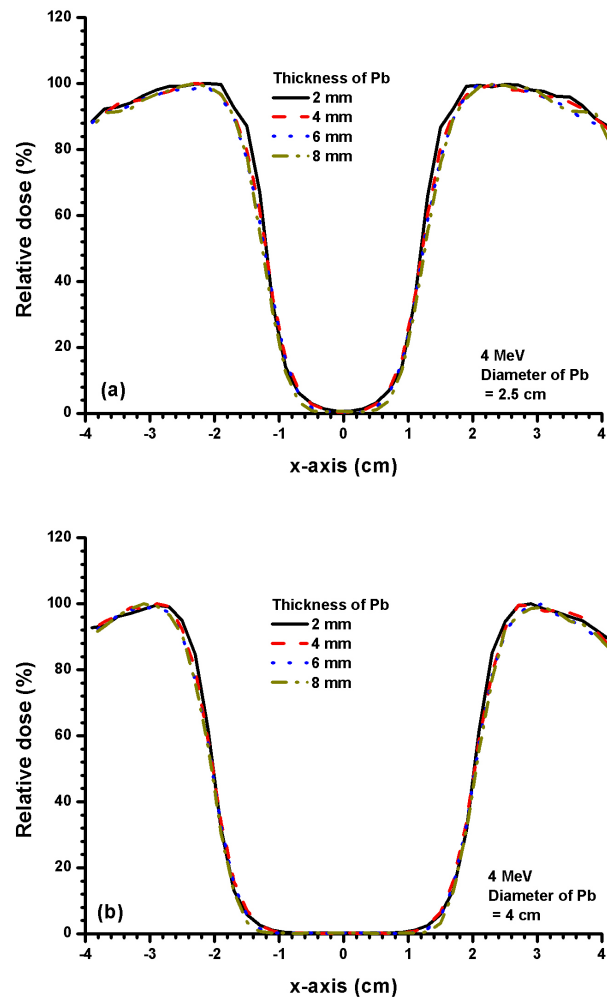


FIG. 6. Beam profiles for Pb layers with diameters of (a) 2.5 and (b) 4 cm and thicknesses of 2, 4, 6 and 8 mm. The 4 MeV electron beams with the $10 \times 10 \text{ cm}^2$ applicator and circular cutout were used. The relative doses at the CAX of all beam profiles for 6(a) and 6(b) were equal to zero.

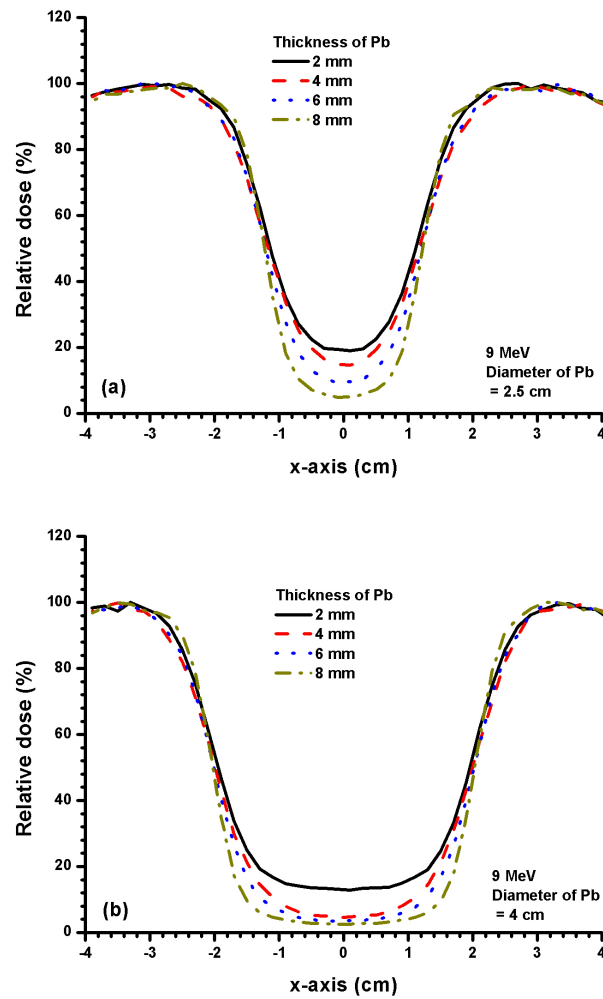


FIG. 7. Beam profiles for Pb layers with diameters of (a) 2.5 and (b) 4 cm and thicknesses of 2, 4, 6 and 8 mm. The 9 MeV electron beams with the $10 \times 10 \text{ cm}^2$ applicator and circular cutout were used. In 7(a), the relative dose at the CAX decreased from 19.3% to 4.8% when the thickness of the Pb layer increased from 2 to 8 mm. When the diameter of the Pb layer is increased to 4 cm (7(b)), the relative dose at the CAX decreased from 13.2% to 3.5% with thickness of the Pb layer increased from 2 to 8 mm.

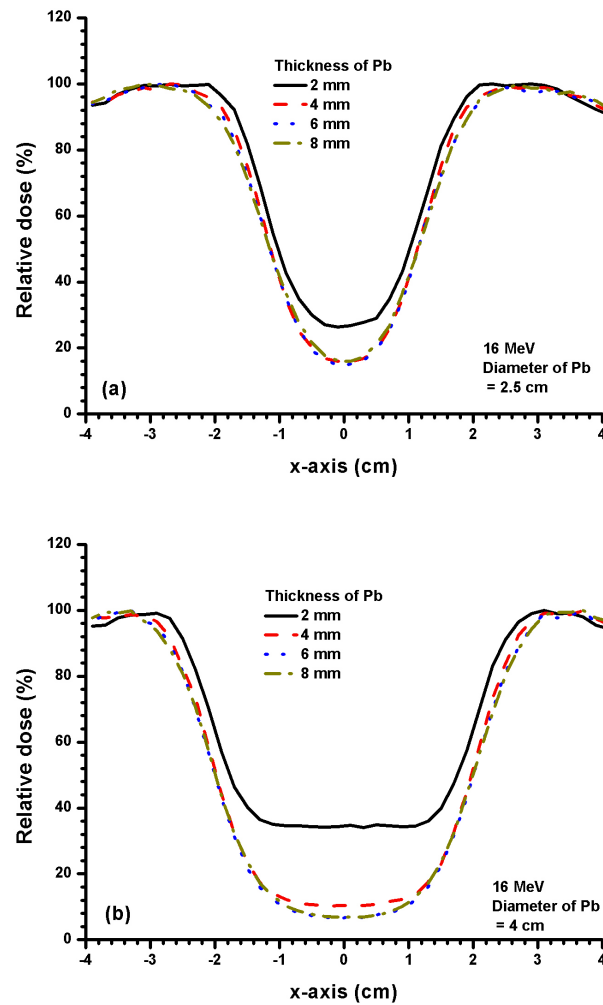


FIG. 8. Beam profiles for Pb layers with diameters of (a) 2.5 and (b) 4 cm and thicknesses of 2, 4, 6 and 8 mm. The 16 MeV electron beams with the $10 \times 10 \text{ cm}^2$ applicator and circular cutout were used. When the thickness of the Pb layer increased from 2 to 8 mm, the relative dose at the CAX decreased from 26.9% to 14.9% for 8(a), and from 34.3% to 6.6% for 8(b).

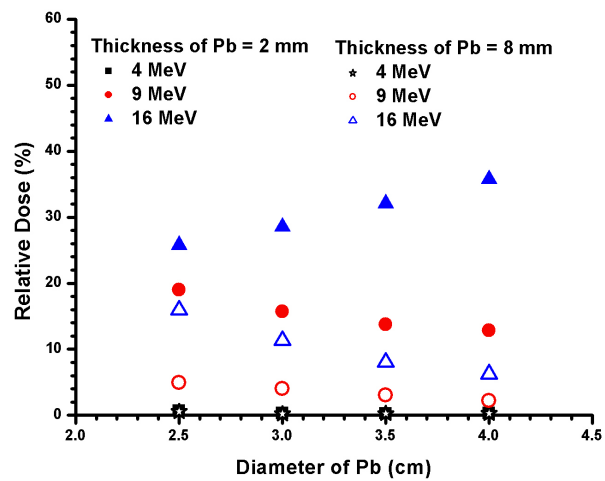


FIG. 9. Relative dose at the CAX vs. diameter of the Pb layer. The 4, 9 and 16 MeV electron beams were used with thickness of Pb equal to 2 and 8 mm. It should be noted that data points for the 4 MeV electron beams with Pb thicknesses of 2 and 8 mm were overlapped in the figure.

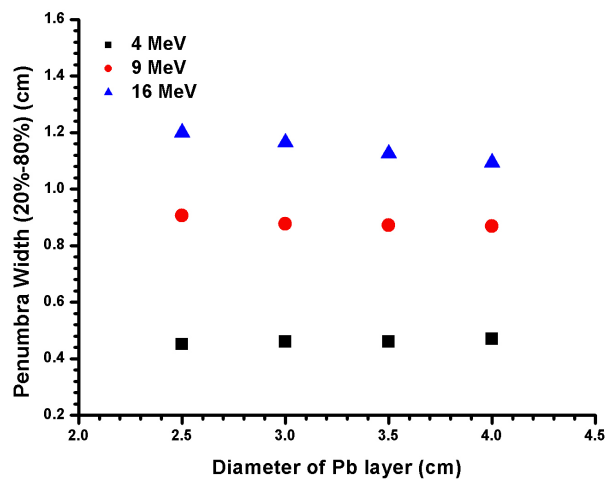


FIG. 10. Penumbra width (20%-80%) at the edge of the Pb layer vs. diameter of the Pb layer for the 4, 9 and 16 MeV electron beams. The beam profiles were measured at 0.7 cm (4 MeV), 2.2 cm (9 MeV) and 3 cm (16 MeV), respectively. The thickness of the Pb layer was equal to 2 mm.

TABLE 1(a): 4 MeV (5HVL)

	<i>Diameter of Pb shield (cm)</i>			
Thickness of Pb	2.5	3.0	3.5	4.0
2 mm	0.39	0.47	0.62	0.67
4 mm	0.43	0.49	0.64	0.68
6 mm	0.47	0.52	0.67	0.70
8 mm	0.52	0.59	0.73	0.76

TABLE 1(b): 9 MeV (4HVL)

	<i>Diameter of Pb shield (cm)</i>			
Thickness of Pb	2.5	3.0	3.5	4.0
6 mm	NA	NA	0.39	0.46
8 mm	0.24	0.41	0.60	0.66

TABLE 1(c): 9 MeV (3HVL)

	<i>Diameter of Pb shield (cm)</i>			
Thickness of Pb	2.5	3.0	3.5	4.0
4 mm	NA	0.27	0.56	0.60
6 mm	0.35	0.48	0.66	0.69
8 mm	0.61	0.64	0.79	0.79

TABLE 1(d): 16 MeV (3HVL)

	<i>Diameter of Pb shield (cm)</i>			
Thickness of Pb	2.5	3.0	3.5	4.0
6 mm	NA	0.11	0.48	0.56
8 mm	NA	0.24	0.50	0.57

Shielding area factors with different thicknesses of Pb for the (a) 4 MeV electron beams with 5 HVL attenuation, (b) 9 MeV electron beams with 4 HVL attenuation, (c) 9 MeV electron beams with 3 HVL attenuation, and (d) 16 MeV electron beams with 3 HVL attenuation. The factors were measured at dm of 0.7, 2.2 and 3 cm for the 4, 9 and 16 MeV electron beams, respectively. The diameter of the Pb layer was equal to 2.5 cm. The percentages on top of each sub-table represent the attenuation result.

IV. DISCUSSION

A. Effect of the Area of the Pb Layer on the Beam Profile

Beam profiles for 2 and 4 mm thickness of Pb with different diameters at d_m can be seen in Figs. 3(a) and 3(b) for the 4 MeV electron beams. It is obvious that both have zero relative doses at the CAX and similar penumbras. Moreover, a 2 mm thickness of Pb is found to be adequate to provide shielding at the CAX. The relative doses at the CAX in Fig. 3 are less than 3% (5 HVL). However, the Pb layer cannot provide the same area of shielding at d_m compared to its physical size because of the finite penumbra width at the edge of the layer.

When the electron beam energy is increased to 9 MeV (Fig. 4), the shielding efficiency is decreased as reflected by the relative dose at the CAX. For example, increasing the thickness

from 2 to 6 mm for a 2.5 cm diameter Pb layer can decrease the relative dose at the CAX from 19.3% to 9.6% (Fig. 4), but it is impossible for the Pb layer to achieve 5 HVL attenuation (Fig. 3). However, it is seen in Fig. 4 that the relative doses at the CAX depend on the diameter of the Pb layer. The larger the Pb layer (from 2.5 to 4 cm diameter with 6 mm thickness) used on the phantom surface, the lower the minimum relative dose (from 9.6% to 3.5% in the beam profile). This is due to the movement of the penumbra at the edge of the Pb layer towards the CAX when the diameter of the layer decreases. Therefore, when the shielding area is decreased, the shielding efficiency for the dose is also decreased because of the penumbra width of the Pb layer. This penumbra width depends on the electron beam energy.

When the electron beam energy is increased to 16 MeV, a 2 mm thickness of Pb can only attenuate the beam to about 30% – 35% at the CAX, depending on the size of the layer (Fig. 5(a)). However, with an 8 mm thickness of Pb reaching the practical shielding limit, the relative dose at the CAX can only be attenuated to about 10% – 15%, which is about 3 HVL at the CAX (Fig. 5(b)). In Fig. 5(a), it is interesting to note that the minimums of the relative dose distribution for diameters of Pb equal to 3.5 and 4 cm extend to both sides of the CAX. This is because of the narrower penumbra width for the high electron beam energy due to a lower scattering cross-section. Therefore, when the shielding area is increased to 3.5 and 4 cm diameter, the two penumbra regions are moved away from the CAX (Fig. 5(a)), resulting in a minimum relative dose region instead of a point. It should be noted that such phenomenon would not happen for thicker Pb layers (Fig. 5(b)) due to a higher attenuation of Pb for the electron beams.

B. Effect of the Thickness of the Pb Layer on the Beam Profile

The dose distribution at d_m does not change significantly with variations in the thickness and diameter of the Pb layer for electron beams with a low energy of 4 MeV. This can be seen in Figs. 6 (a) and (b). All beam profiles do not change significantly when the small (2.5 cm diameter, Fig. 6(a)) and larger (4 cm diameter, Fig. 6(b)) Pb layers were used with different thicknesses. The profiles show that for low-energy electron beams, the diameter and thickness of the Pb layer would not affect the dose distribution at d_m . In addition, a 2 mm thickness of Pb is seen to be adequate for shielding (Fig. 6).

However, for the higher electron beam energy of 9 MeV with a small Pb layer (2.5 cm diameter), the beam profile and relative dose at the CAX depend on the thickness of the Pb layer (Fig. 7(a)). The thicker the layer used in the calculation, the lower the relative dose at the CAX. The relative doses at the CAX changed from 20% to 5% when Pb layers with thicknesses of 2 – 8 mm were used for shielding. When a larger Pb layer (4 cm diameter) was used, the change of relative dose at the CAX was different from that of the smaller diameter layer. In Fig. 7(b), the relative dose at the CAX for the 2 mm thickness of Pb is about 13%; however, the relative dose is decreased significantly (from 5% to 3%) when the thickness of Pb is increased from 4 – 8 mm. Compared to Fig. 6, it is obvious from Fig. 7 that 2 mm of Pb is not adequate to attenuate the electron beam efficiently. However, when the thickness of the Pb layer is increased to 4 mm, the beam attenuation can be improved from 14% to 5%.

Similar effects of Pb thickness on the relative dose at the CAX are seen in Fig. 8. For 16 MeV electron beams, the relative doses at the CAX for 2 mm thickness of Pb layers with diameters of 2.5 cm (Fig. 8(a)), and 4 cm (Fig. 8(b)) are equal to 27% and 37%, respectively. The higher relative dose for the larger Pb layer is due to the increase of the photon contamination of the 16 MeV electron beams compared to 4 and 9 MeV.^(31,32) It is seen that 8 mm thickness of Pb cannot provide greater than 3 HVL attenuation for a Pb layer with 4 cm diameter using the 16 MeV electron beams.

C. Relative Dose at the CAX and d_m

The relative dose at the CAX and d_m reflects the attenuation of the electron beam due to the presence of the Pb layer. As discussed in Sections IV. A and IV. B above, this dose depends on the electron beam energy, size and thickness of the Pb layer. These dependencies are not significant for low electron beam energy such as 4 MeV (Fig. 9). For electron beams with energy of 9 MeV, the relative dose slightly decreases with increase of diameter of the Pb layer. This is because of a decrease of the side scatter contribution to the CAX, as the distance between the edge of the Pb layer and the CAX increases.^(33,34) In Fig. 9, it can be seen from the 9 MeV electron beams that increasing the thickness of the Pb layer from 2 to 8 mm increases the attenuation by 10% – 13%.

When the electron beam energy is increased to 16 MeV, the relative dose at the CAX is found to decrease with the diameter of the Pb layer for a thickness of 8 mm. The reason is similar to that for the 9 MeV electron beam. However, when the thickness of the Pb layer is decreased to 2 mm, it is seen that the relative dose at the CAX increases (from 26.5% to 34.5%) with an increase of the diameter of the Pb layer (from 2.5 to 4 cm) for the 16 MeV electron beams. This is because (1) the higher penetration power of the 16 MeV electron beams allows more electrons to pass through the 2 mm of Pb, and (2) such a thin Pb layer acts as a source of photon contamination and scattering medium.^(31,32)

D. Penumbra Width Varying With the Diameter of the Pb Layer

Figure 10 shows the penumbra width (20% - 80%) for different diameters of the Pb layer with 2 mm thickness and the 4, 9 and 16 MeV electron beams. It is seen that the penumbra width increases with the electron beam energy, and does not vary significantly with the diameter of the Pb layer for the 4 and 9 MeV electron beams. However, for the 16 MeV electron beams, the penumbra width decreases slightly with the diameter of the Pb layer. This is because for high electron beam energies, increased side scattering contributes more dose to the CAX.^(33,34) This increases the dose in the low-dose region in the penumbra, resulting in a larger penumbra width. This effect is more significant for a smaller Pb layer as the edge of the shield is closer to the CAX at d_m .

E. Shielding Area Factor

In electron radiotherapy, it is well known that a larger area of Pb compared to the size of the critical tissue should be used for shielding due to the side scatter of the electron beam. The actual size of the Pb layer, based on the size of the critical tissue at d_m , depends on the electron beam energy and dimensional characteristics of the Pb shield. A parameter called shielding area factor (Eq. 2) is introduced to predict the actual size of the Pb layer used for shielding.

Table 1 shows the shielding area factors for the 4, 9 and 16 MeV electron beams with different thicknesses and diameters of Pb. Using the 4 MeV electron beams (Table 1(a)), 5 HVL attenuation can easily be achieved. It can be seen that the shielding area factor increases with the area of the Pb shield, reflecting that a larger shielding area, compared to the shielded volume, is needed. For 9 MeV electron beams (Tables 1(b) and 1(c)), less than 5 HVL attenuation can be achieved using up to an 8 mm thickness of Pb. The attenuation is lowest for the 16 MeV electron beams, and only 3 HVL can be achieved. From Table 1, it can be seen that the efficiency of shielding is decreasing with a reduction of thickness and size of the Pb layer, in particular for the high-energy electron beam (16 MeV). This dosimetric data is useful for radiation oncology staff in predicting the dimension of the Pb layer for shielding before the treatment planning and dose calculation.

V. CONCLUSIONS

For the variation of diameter of the Pb layer, the doses at the CAX and penumbra widths at the edge of the layer and d_m did not change significantly for the 4 MeV electron beams. When higher electron beam energies (9 and 16 MeV) were used, the dose at the CAX increased with the electron beam energy for the same thickness of Pb. For the same diameter of the Pb layer, 2 mm thickness was found to be adequate to provide shielding with 5 HVL attenuation for the 4 MeV electron beams. However, with higher electron beam energies of 9 and 16 MeV, only 4 and 3 HVL attenuation could be achieved by using 8 mm of Pb.

It was found that the beam profile at d_m depends on: (1) the penumbra at the edge of the Pb layer; (2) the electron beam attenuation due to the Pb layer; (3) the electron side scatter contributing to the dose at the CAX; and (4) the photon contamination produced by the Pb for different electron beam energies. Points 1 through 4 are related to the size and thickness of the Pb layer and, therefore, it is concluded that the dosimetry at d_m depends on the dimensional characteristics of the Pb layer.

The shielding area factor defined in this study was proposed to estimate the shielding effect of the Pb layer varying with its dimension. This factor is important to help the radiation oncology staff decide the size and thickness of the Pb layer prior to the computer treatment planning and dose calculation in the electron radiotherapy.

ACKNOWLEDGEMENTS

JCLC would like to thank Dr. David Jaffray for his support in the Monte Carlo simulation at the Princess Margaret Hospital. The measurements using radiographic films were carried out in the Grand River Hospital. JCLC would also like to thank Varti Vartanian and Mitch Spiegel of Varian Medical Systems for providing detailed information of the 21 EX Linac when using electron beams, and Dr. Frank Verhaegen of McGill University for sharing his BEAMnrc input files for verification of the electron beam simulation. The assistance of Julia Publicover in proofreading this manuscript is appreciated.

REFERENCES

1. Saunders JE, Peters VG. Back-scattering from metals in superficial therapy with high energy electrons. *Br J Radiol.* 1974;47(560):467–70.
2. Shiu AS, Tung SS, Gastorf RJ, Hogstrom KR, Morrison WH, Peters LJ. Dosimetric evaluation of lead and tungsten eye shields in electron beam treatment. *Int J Radiat Oncol Biol Phys.* 1996;35(3):599–604.
3. Weaver RD, Gerbi BJ, Dusenbery KE. Evaluation of eye shields made of tungsten and aluminum in high-energy electron beams. *Int J Radiat Oncol Biol Phys.* 1998;41(1):233–37.
4. Perez-Calatayud J, Ballester F, Serrano MA, Lluch JL, Casal E, Carmona V. Dosimetric characteristics of back-scattered electrons in lead. *Phys Med Biol.* 2000;45(7):1841–49.
5. Klevenhagen SC, Lambert GD, Arbabi A. Backscattering in electron beam therapy for energies between 3 and 35 MeV. *Phys Med Biol.* 1982;27(3):363–73.
6. Weatherburn H, McMillan KTP, Stedeford G, Durrant KR. Physical measurements and clinical observations on the backscatter of 10 MeV electrons from lead shielding [letter]. *Br J Radiol.* 1975;48(567):229–230.
7. Khan FM, Moore VC, Levitt SH. Field shaping in electron beam therapy. *Br J Radiol.* 1976;49(586):883–86.
8. Gagnon WF, Cundiff JH. Dose enhancement from backscattered radiation at tissue-metal interfaces irradiated with high energy electrons. *Br J Radiol.* 1980;53(629):466.
9. Lambert GD, Klevenhagen SC. Penetration of backscattered electrons in polystyrene for energies between 1 and 25 MeV. *Phys Med Biol.* 1982;27:721–725.
10. Das IJ, Cheng CW, Mitra RK, Kassaei A, Tochner Z, Solin LJ. Transmission and dose perturbations with high-Z materials in clinical electron beams. *Med Phys.* 2004;31(12):3213–21.
11. Chow JCL, Grigorov GN. Monte Carlo simulation of backscatter from lead for clinical electron beam using EGSnrc. *Med Phys.* 2008;35(4):1241–50.
12. Kronenberg SJ, Brucker GJ. The use of hydrogenous material for sensitizing pMOS dosimeters to neutrons. *IEEE Trans on Nucl Sci.* 1995;42(1):20–26.

13. Rosenfeld AB, Siegbahn EA, Brauer-Krish E, et al. Edge-on face-to-face MOSFET for synchrotron microbeam dosimetry: MC modeling. *IEEE Trans on Nucl Sci.* 2005;52(6):2562–69.
14. Chow JCL, Newman S. Experimental verification of the application of lateral buildup ratio on the 4-MeV electron beam. *J Appl Clin Med Phys.* 2006;7(1):35–41.
15. Chow JCL, Grigorov GN. Electron radiotherapy: a study on dosimetric uncertainty using small cutouts. *Phys Med Biol.* 2007;52(1):N1–11.
16. Chow JCL. Calculation of lateral buildup ratio using Monte Carlo simulation for electron radiotherapy. *Med Phys.* 2007;34(1):175–82.
17. Nelson WR, Hirayama H, Rogers DWO. The EGS4 code system, SLAC Report 265. Stanford, CA: Stanford Linear Accelerator Center; 1985.
18. Kawrakow I, Rogers DWO. The EGSnrc code system: Monte Carlo simulation of electron and photon transport. NRCC Technical Report PIRS-701. Ottawa, Canada: National Research Council of Canada; 2000.
19. Rogers DWO, Faddegon BA, Ding GX, Ma CM, We J, Mackie TR. BEAM: a Monte Carlo code to simulate radiotherapy treatment units. *Med Phys.* 1995;22(5):503–24.
20. Rogers DWO, Ma CM, Ding GX, et al. BEAMnrc users manual. NRC Report PIRS 509b(revF). Ottawa, Canada: National Research Council of Canada; 2001.
21. Ma CM, Reckwerdt P, Holmes M, Rogers DWO, Geiser B. DOSXYZ user manual, NRC Report PIRS 509b. Ottawa, Canada: National Research Council of Canada; 1995.
22. Brahme A, Svensson H. Specification of electron beam quality from the central-axis depth absorbed dose distribution. *Med Phys.* 1976;3(2):95–102.
23. American Association of Physicists in Medicine. RTC Task Group 21: A protocol for the determination of absorbed dose from high-energy photon and electron beams. *Med Phys.* 1983;10(6):741–71.
24. Rogers DWO, Bielajew AF. Differences in electron depth-dose curves calculated with EGS and ETRAN and improved energy-range relationships. *Med Phys.* 1986;13(5):687–94.
25. Khan FM. The physics of radiation therapy. 3rd ed. Philadelphia (PA): Lippincott Williams and Wilkins; 2003.
26. Chow JCL, Grigorov GN. Effect of electron beam obliquity on lateral buildup ratio: a Monte Carlo dosimetry evaluation. *Phys Med Biol.* 2007;52(13):3965–77.
27. Bielajew AF, Rogers DWO. PRESTA-The Parameter Reduced Electron-step Transport Algorithm for Electron Monte Carlo Transport. *Nucl. Instrum. Part B. Nucl Med & Biol.* 1984;18:535–48.
28. Mainegra-Hing E, Rogers DWO, Kawrakow I. Calculation of photon energy deposition kernels and electron dose point kernels in water. *Med Phys.* 2005;32(3):685–99.
29. Almond PR, Biggs PJ, Coursey BM, et al. AAPM's TG-51 protocol for clinical reference dosimetry of high energy-photon and electron beams. *Med Phys.* 1999;26(9):1847–70.
30. Chow JCL, Grigorov GN. Peripheral dose outside applicators in electron beams. *Phys Med Biol.* 2006;51(12):N231–40.
31. Sorcini BB, Hyödynmaa S, Brahme A. Quantification of mean energy and photon contamination for accurate dosimetry of high-energy electron beams. *Phys Med Biol.* 1997;42(10):1849–73.
32. Jeraj R, Keall PJ, Ostwald PM. Comparisons between MCNP, EGS4 and experiment for clinical electron beams. *Phys Med Biol.* 1999;44(3):705–17.
33. Zhang GG, Rogers DWO, Cygler JE, Mackie TR. Monte Carlo investigation of electron beam output factors versus size of square cutout. *Med Phys.* 1999;26(5):743–50.
34. Boyd RA, Hogstrom KR, White RA, Starkschall G. Modelling pencil-beam divergence with the electron pencil-beam redefinition algorithm. *Phys Med Biol.* 2001;46(11):2841–56.